Paper published in 2026 IEEE Trans. Appl. Supercond. 36 8200206
DOI: 10.1109/TASC.2025.3646984

Magnetic screening behavior of hybrid high-temperature superconducting screens subjected to successive excitation cycles: experiments and numerical study

Nicolas Rotheudt, Jean-François Fagnard, Tomas Hlasek, Jan Plechacek and Philippe Vanderbemden

***Abstract*—Combining high-temperature superconducting bulks and jointless closed-loop coated conductors recently demonstrated promising magnetic shielding/screening properties when they are zero-field cooled and subjected to an inhomogeneous applied field. The present work focuses on studying how their screening properties evolve if several magnetic field excitation cycles are applied, as it is the case in practical applications. This study is carried out both experimentally and numerically. The main result is that more than 95% of the field attenuation (screening factor SF) obtained after the first ramp still remain after 300 cycles. This result is explained by using the numerically computed current density distribution in the bulk alone. The slight decrease in SF after several cycles is found to be smaller than the field attenuation arising from conventional current relaxation (or flux creep) if the magnetic field is kept constant after the first increasing ramp. These results demonstrate the potential of such superconducting screens for practical applications with a large number of excitation applied field cycles.**

***Index Terms*—Magnetic shielding, shielding, large-scale applications, coated conductors, bulk conductors, HTS coils, magnetic field measurement.**

I. Introduction

SEVERAL engineering applications involving large magnetic flux densities require their low frequency stray field to be reduced to protect neighboring equipment, e.g., large superconducting magnets or air-core superconducting machines [1]–[3]. The present work deals with passive systems based on high-temperature superconductors (HTS) to provide the required field attenuation [4]. These systems can be referred to as magnetic shields (closed or partly closed geometry surrounding the attenuated zone) or screens (open geometry), on which we focus here. When the applied field varies, persistent currents are naturally induced in the superconductors to counteract this field, providing attenuation on the other side of the screen as shown in Fig. 1. Fig. 1 illustrates that a magnetic screen can consist of a bulk superconductor alone, a set of closed-loop (jointless) coils [5], [6] or a 'hybrid' screen combining both, which recently demonstrated superior screening ability [7], [8].

N. Rotheudt, J.-F. Fagnard and P. Vanderbemden are with the Department of Electrical Engineering and Computer Science, University of Liège, Liège, Belgium.
T. Hlasek and J. Plechacek are with CAN SUPERCONDUCTORS, s.r.o., Kamenice, Czech Republic.
T. Hlasek is with the Department of Inorganic Chemistry, University of Chemistry and Technology, Prague, Czech Republic.
This work was supported by the Fonds de la Recherche Scientifique-FNRS under Grant CDR n°J.0184.23. N. Rotheudt is recipient of an FRS-FNRS Research Fellow Grant. The work of T. Hlasek was supported by the Czech Science Foundation (Project 24-10171S).

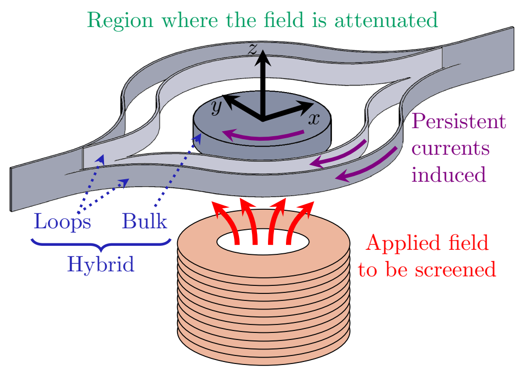

Fig. 1. Schematic illustration of a magnetic screening experiment for different types of HTS screens. The reference axes used in this work are shown. Adapted from N Rotheudt *et al.* 2025 *Supercond. Sci. Technol.* **38** 025012 [8], figure 2. © IOP Publishing. Reproduced with permission. All rights reserved.

The performance of a magnetic screen, i.e., the field attenuation, is assessed through the screening factor $\mathrm{SF}(\boldsymbol{r}) = \mu_0 H_{\mathrm{app}}(\boldsymbol{r})/B(\boldsymbol{r})$, where $\boldsymbol{r}$ is a certain position, $\mu_0 H_{\mathrm{app}}$ the magnitude of the applied field (without HTS screen) and B the magnitude of the flux density with the screen. In the magnetic shielding or screening studies carried out in the literature [4], the superconductors are first zero-field cooled and then subjected to a field ramped up from 0 to $H_{\max}$. In practical applications, however, a screen is subjected to several applied field cycles ($0 \rightarrow H_{\max} \rightarrow 0$). It is therefore desired to investigate whether the magnetic screening properties after the first ramp are maintained for several field cycles, in spite of the hysteretic nature of type-II superconductors. Interestingly, for magnetic shields such as long tubes, a full penetration field H_p can be clearly defined [9]. Hence, if $H_{\max} \ll H_p$, no measurable effect results from the application of several field cycles [10]. The situation is less clear for magnetic screens (Fig. 1) for which SF behind the screen depends on the flux lines meandering around the superconductors.

In this paper, we investigate the behavior of HTS magnetic screens subjected to repeated cycles of the applied field.

II. Experimental set-up and results

The superconducting screen is placed above a source coil generating an inhomogeneous field. Details about the source coil and the sample holders are given in our previous works [7], [8]. A bespoke cryogenic 3-axis Hall probe [11] is fixed to a xyz micro-displacement system and measures simultaneously B_x, B_y and B_z above the screen. The Hall probe consists of a room-temperature 3-axis Hall sensor placed inside a thermally controlled G10 insert. As a result, the active area of the Hall sensor is located at 2.2 ± 0.25 mm from the bottom surface of the insert, which determines the minimal distance from the bulk at which measurements can be performed.

The HTS screen is first zero-field cooled down to 77 K. Then, the current in the coil is slowly ramped up to 0.5 A in 100 s. Note that 0.5 A in the coil corresponds to an inhomogeneous applied field (without superconductor) whose peak value at the center of the bottom surface of the screen is around 100 mT. After 300 s at 0.5 A to ensure that the results are sufficiently weakly time dependent [7], the spatial distribution of B_x, B_y and B_z is measured above the screen every 0.5 mm along y. At each point, 6 measurements sent by the Hall probe are averaged (these measurements themselves being the result of an average of 100 internal readings [11]). Once the flux density mappings are performed, the current in the coil is decreased to 0 at the same sweep rate (5 mA/s). This cycle 'increase – mapping – decrease' is done 30 times and the resulting mappings of SF at 0.5 A are compared. This is in sharp contrast with [7], [8], where we studied in detail a single increasing ramp of applied field.

Two HTS screens are investigated. The first screen is a disk-shaped melt-textured GdBCO/Ag bulk alone (thickness 5 mm, diameter 30 mm, $J_\mathrm{c}(77\ \mathrm{K}) \approx 200\ \mathrm{A\ mm}^{-2}$), which is produced by the 'single-direction melt growth' (SDMG) method [12]–[14] at CAN Superconductors, s.r.o. The second screen is a hybrid screen combining this bulk sample with 45 mm- and 60 mm-diameter closed-loop coated conductors [7], [8]. These are jointless superconducting loops obtained by milling a slit in the middle of a tape segment [15]–[20]. The tape segments are from a 10 mm-wide 2G GdBCO tape from Shanghai Superconductor Technology ($I_\mathrm{c}(77\ \mathrm{K},\ \mathrm{s.f.}) \approx 500$ A) and the slit is positioned at the same height as the top surface of the bulk, i.e., at $z = 0$. To increase the total field that can be generated by these loops, 4 non-insulated layers are superimposed for each loop. The 45 mm- and 60 mm-diameter closed loops are oriented with the vertical offset on the same side of the bulk (see Fig. 1). It is worth mentioning that a magnetic screen consisting of the loops alone is not well-suited for the type of inhomogeneous applied field considered in this work. The reason, explained in [7], is the following. On the one hand, the amplitude of the applied field is maximum at $y = 0$. On the other hand, when screening currents are induced in the loops, the field generated by these currents is rather small at the center, and maximum close to the superconducting tape. Hence, a magnetic screen made of the loops alone is not effective since the spatial distribution of the opposite field generated by these loops differs strongly from the spatial distribution of the applied field. Such a screen will, therefore, not be considered in this paper.

Fig. 2 shows the SF measurements along y (from $y = -43$ mm to $y = 12$ mm) at $z = 4.7$ mm (see Fig. 1), i.e. when the bottom of the G10 insert of the Hall probe is at 2.5 mm above the bulk. Each set of curves shows 4 different SF mappings and corresponds to a given screen: either the 'bulk alone' or the 'hybrid' screen. The mapping results given in Fig. 2 are measured during the 1^{st}, 10^{th}, 20^{th} and 30^{th} cycle 'increase field – mapping – decrease field' and are labeled M. 1, M. 10, M. 20 and M. 30, respectively. The main observation is that, for each screen, the different SF mappings are similar. It can be shown that the minor variations from one mapping to another corresponds to B variations around a few dozen µT, which is smaller than the typical uncertainty level of the Hall probe (~ 100 µT [11]). Therefore, these results give evidence that the screening properties obtained after the first ramp of applied field to H_max are globally maintained at each subsequent occurrence of H_max (up to 30 cycles), in spite of the hysteretic nature of the superconductors. In the following, a finite element model is used to (i) understand these results, and (ii) extend this conclusion to higher fields and for a much larger number of cycles.

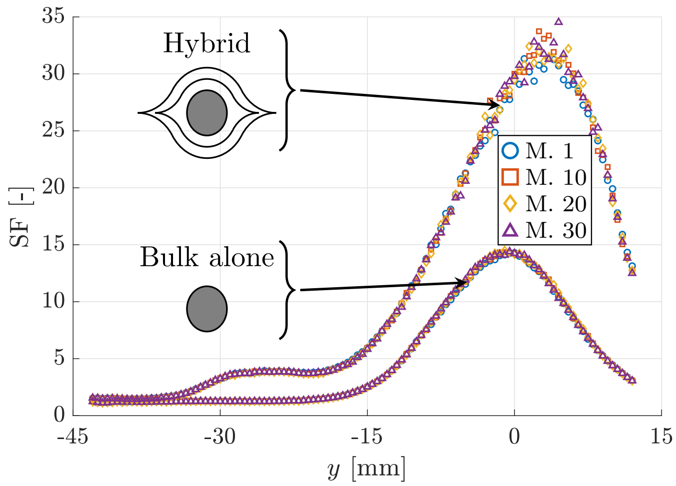

Fig. 2. Spatial distribution of SF along y at $z = 4.7$ mm above the top surface of the bulk. The bottom set of curves is for a screen made of the bulk alone. The top set of curves is for the hybrid screen (bulk alone with 45 mm- and 60 mm-diameter closed-loop coated conductors). Each set of curves consists of 4 curves corresponding to 4 out of the 30 SF mappings (M. i stands for the i-th mapping).

Another observation in Fig. 2 is that the SF measurements are not centered around $y = 0$. As explained in [7], [8], this is because of the offset between both halves of the loop: the distance to the loop for $y > 0$ is smaller than for $y < 0$ (see Fig. 1). Consequently, the opposite field generated by the currents in the loops is larger for $y > 0$ than the field generated for $y < 0$, leading to a higher SF for $y > 0$.

III. Finite Element Model and Results

In our previous work, we demonstrated that a simple 2D finite element model using axisymmetry can be used to understand most screening properties on both bulk and hybrid screens [8]. This model is implemented in the Gmsh and GetDP environments with the Life-HTS toolkit [21]. The characteristics of the bulk are those described in section II (constant J_c assumed) and the power law exponent [22] is $n = 40$ in this section. To ease the meshing of the domains, the thickness of the

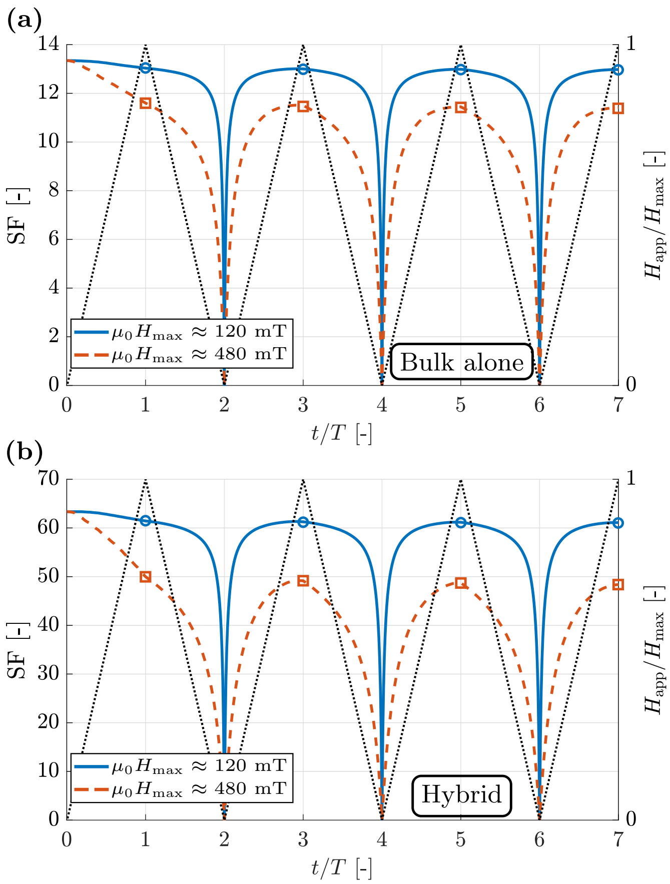

Fig. 3. Time evolution of SF at $(y, z) = (0, 4.7)$ mm for the first cycles of two field amplitudes with the same sweep rate: 1.2 mT/s at the bottom of the screen which consists of **(a)** the bulk alone or **(b)** the bulk and the loops (hybrid screen). First case (plain blue curve): up to $\mu_0 H_{max} \approx 120$ mT at the bottom of the bulk ($T = 100$ s). Second case (dashed red curve): up to $\mu_0 H_{max} \approx 480$ mT ($T = 400$ s). The dotted black curve shows the relative evolution of H_{app} up to H_{max}. The blue circles and red squares indicate the SF values when $H_{app} = H_{max}$.

two loops (45 and 60 mm-diameter) is artificially increased to 1 mm. The $H - \phi$ formulation is used [23], [24]. The current in the source coil, hence the applied field, varies linearly with time, repeating 300 times the sequence $0 \rightarrow H_{max} \rightarrow 0$.

A. Detailed time evolution for the first cycles

Fig. 3 compares the time evolution of SF at 4.7 mm above the center of **(a)** the bulk screen and **(b)** the hybrid screen for the first cycles of applied field in two cases. In the first case (plain blue curve), the field at the center of the bottom surface of the bulk goes up to $\mu_0 H_{max} \approx 120$ mT in $T = 100$ s, i.e., the sweep rate is 1.2 mT/s. This applied field is roughly equivalent to the experimental one. In the second case (dashed red curve), $\mu_0 H_{max} \approx 480$ mT using the same sweep rate (hence, $T = 400$ s). The dotted black curve shows the relative time evolution of the applied field.

The first observations, which hold both for Fig. 3**(a)** and Fig. 3**(b)**, are for $t/T \leq 1$. At $t/T \rightarrow 0$, SF is the same for both curves, since it is dictated by the geometry of the screen [8]. Then, for $0 < t/T \leq 1$, i.e., when H_{app} first increases, SF decreases. This phenomenon is due to the flux front penetrating deeper in **(a)** the bulk or **(b)** the bulk and the loops when the applied field increases, as illustrated for the bulk alone in section III-B. In Fig. 3**(a)**, SF drops by $\sim 2.3\%$ for $\mu_0 H_{max} \approx 120$ mT and by $\sim 13\%$ for 480 mT. In Fig. 3**(b)**, SF drops by $\sim 3\%$ for $\mu_0 H_{max} \approx 120$ mT and by $\sim 21\%$ for 480 mT. Solutions to limit this SF degradation involve lowering the operating temperature or combining several superconductors [8].

Then, the SF obtained at each occurrence of H_{max}, indicated by the blue circles and the red squares in Fig. 3, is similar, as highlighted experimentally in section II. From $t/T = 1$ to $t/T = 7$ and for $\mu_0 H_{max} \approx 120$ mT, SF decreases by $\sim 0.4\%$ for the bulk alone and by $\sim 0.5\%$ for the hybrid screen. For 480 mT, from $t/T = 1$ to $t/T = 7$, SF decreases by $\sim 1.7\%$ for the bulk alone and by $\sim 3.2\%$ for the hybrid screen. Hence, even for fields larger than those used experimentally, the screening properties are expected to be maintained over a few excitation cycles.

Also, it can be noticed that the SF values obtained using the axisymmetric finite element model are significantly larger than the experimental ones. The two main reasons are: (i) the flux density measured above the screen is relatively small, such that the typical uncertainty level of the Hall probe prevents us from measuring flux densities ≤ 100 µT, and (ii) the vertical offset between both halves of the loops leads a finite B_y in practice, hence a limited SF. Symmetrizing the design by reversing the direction of one of the loops can increase the experimental SF [8].

In the following sections, for the sake of simplicity and conciseness, we focus on a screen consisting of the bulk alone, but the conclusions also hold for hybrid screens.

B. Explanation using the current density distribution

Studying how the current density J distribution evolves with the applied field cycles is very helpful to understand the results of section III-A. Fig. 4 shows the J distribution in half of the cross-section of the bulk (axisymmetric model – screen consisting of a bulk alone). This J distribution is drawn at selected time instants taken from the dashed red curve in Fig. 3**(a)** ($\mu_0 H_{max} \approx 480$ mT at the center of the bottom of the bulk, sweep rate 1.2 mT/s, bulk alone), which is replicated for visual purposes in Fig. 4.

For $0 < t/T \leq 1$, a flux front penetrates in the bulk, starting from its edges and where the field is the most concentrated. Consequently, a current density is induced (cross-section 1 in Fig. 4). The higher H_{max}, the deeper the flux front in the bulk. At $t/T = 1$, a certain current density is therefore induced up to a given depth (cross-section 2). For $1 < t/T \leq 2$, new currents arise from the edges in the opposite direction and 'erase' part of those already flowing in the bulk (cross-sections 3 and 4). Then, for $2 < t/T \leq 3$, new currents erase those in the opposite direction starting from the edges (cross-section 5), and it can be observed that the current density distribution at $t/T = 3$ (cross-section 6) is very close to that at $t/T = 1$. Similar observations hold for $t/T = 5$ and $t/T = 7$ (cross-sections 7 and 8).

In the framework of the critical state model ($n \rightarrow \infty$) [25], the new currents that are created from the edges at each

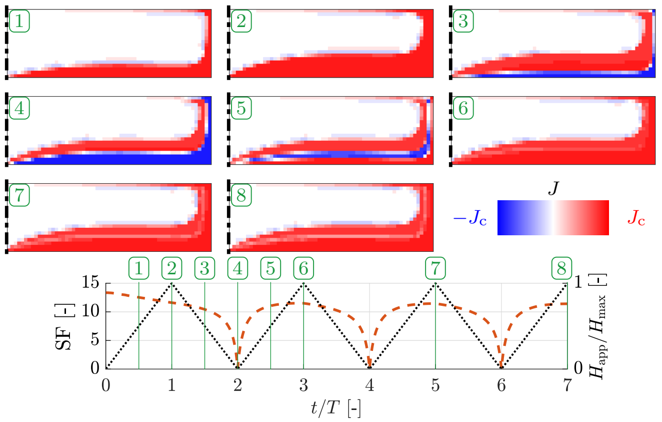

Fig. 4. Bottom: time evolution of SF at $(y, z) = (0, 4.7)$ mm for $\mu_0 H_{\max} \approx 480$ mT, replicated from Fig. 3 for reference. Top: current density J distribution in the bulk for the time instants indicated on the bottom graph. Only half of the cross-section is shown by symmetry. The color map represents J, ranging from $-J_c$ to $J_c = 200$ A/mm^2 (assumed to be constant).

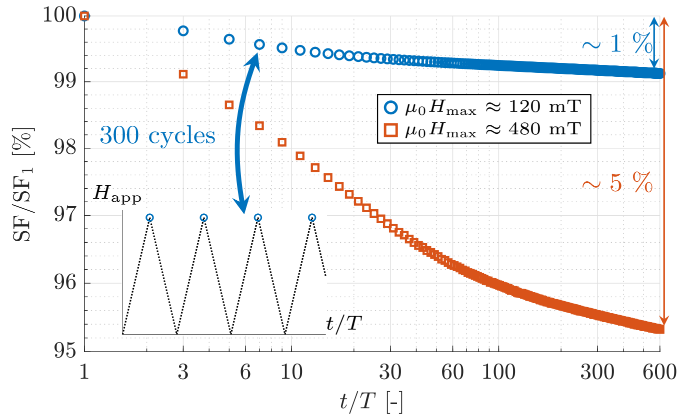

Fig. 5. Relative time evolution of SF at $(y, z) = (0, 4.7)$ mm over 300 cycles of applied field in two cases (screen made of the bulk alone). First case (blue circles): applied field up to $\mu_0 H_{\max} \approx 120$ mT at the bottom of the bulk ($T = 100$ s). Second case (red squares): applied field up to $\mu_0 H_{\max} \approx 480$ mT ($T = 400$ s). Only the SF values when $H_{\rm app} = H_{\max}$ are shown, as indicated in the inset. The reference SF$_1$ is SF$(t/T = 1)$. The axes are in logarithmic scale.

reversal of $\mathrm{d}H_{\rm app}/\mathrm{d}t$ will never penetrate deeper than the given depth reached at $t/T = 1$. For real superconductors (finite n), the J distribution is similar but the penetration front moves very slightly to the center of the bulk and the average J decreases very slowly due to the current relaxation (flux creep), as detailed in section IV.

C. Evolution of SF for 300 excitation cycles

In practical applications, a magnetic screen will experience more than a few cycles after being cooled down. We therefore investigate, for the bulk screen, how the SF value for $H_{\rm app} = H_{\max}$ evolves over much longer runs, e.g., 300 cycles. Fig. 5 shows SF at $z = 4.7$ mm for each occurrence of $H_{\max}$, as shown in the inset, relatively to the SF$(t/T = 1) = $ SF$_1$. For $\mu_0 H_{\max} \approx 120$ mT (blue circles), SF decreases by less than 1% over 300 cycles; for $\mu_0 H_{\max} \approx 480$ mT (red squares), less than 5%. This very low reduction of SF with the number of cycles (log scale) confirms that the screening properties obtained after the first ramp of applied field are maintained over long runs.

Since this slow decay resembles what is observed in trapped field experiments due to current relaxation [26], section IV compares the two phenomena.

IV. Discussion

Two families of applied field are considered: (i) the 'cycles' case, as described before and (ii) the 'relaxation' case, where $H_{\rm app}$ is first ramped up to $H_{\max}$ in T seconds (same sweep rate in both cases) then kept constant. In the 'relaxation' case, a certain J is induced in the bulk for $t/T \leq 1$ and only current relaxation (or flux creep) occurs for $t/T > 1$. According to Zeldov's model [27], this relaxation writes [22]

$$J(t) \approx J(0) \left[1 - \frac{1}{n} \ln\left(\frac{t}{\tau_0}\right)\right], \tag{1}$$

for $t \gg \tau_0$. For a fully penetrated sample, this equation shows that the relaxation rate $\mathrm{d}M/\mathrm{d}\ln(t)$, M being the magnetic moment of the sample, scales as $1/n$. However, the bulk sample is *not* fully penetrated in this work and Babich *et al.* [28] showed that less-penetrated samples are characterized by a smaller relaxation rate. Consequently, if $H_{\max}$ is higher, the flux front penetrates more deeply and the relaxation rate is larger. In this case, J, hence SF, decreases faster, as highlighted in Fig. 5. Also, in addition to this overall J decay, the penetration front slowly drifts deeper in the bulk.

Fig. 6 shows the relative decrease of SF at each occurrence of $H_{\max}$ in the 'cycles' case (open symbols, see the inset of Fig. 5) and in the 'relaxation' case at the same time instants (full symbols, see left inset of Fig. 6). In both cases, $\mu_0 H_{\max} \approx 480$ mT ($T = 400$ s) and $n = 40$ (red squares, same as in Fig. 5) and 20 (green triangles) are compared.

In the 'relaxation' case, it is expected that the smaller the n, the faster the average J decrease, given (1), even in a partially penetrated bulk. Hence, even though SF depends on both the average J in the bulk and the precise J distribution, a smaller n yields a faster decay of SF. Note that, in practice, a different n value is accompanied by a different J reorganization over time, such that the decrease rate of SF does not exactly match that of the average J. Interestingly, it can be observed in Fig. 6 that n also influences the SF decay in the 'cycles' case: SF decreases more rapidly for smaller n, which provides evidence that this SF decay is intrinsically related to conventional current relaxation.

For $n = 20$, Fig. 6 illustrates that the decrease of SF in the 'cycles' case is smaller than in the 'relaxation' case. For $n = 40$, few differences between both cases appear after 300 cycles but the right inset highlights that, again, the decay caused by the cycles is smaller than conventional relaxation, beyond 300 cycles (crossover at $t/T \approx 341$). This confirms that the screening properties are maintained over long runs of applied field cycles. By neglecting the spatial evolution of the J distribution and assuming that SF only depends on the average J, given by (1), this fact can be explained as follows.

Each time $\mathrm{d}H_{\rm app}/\mathrm{d}t$ changes sign ('cycles' case), new currents appear in the opposite direction (see section III-B)

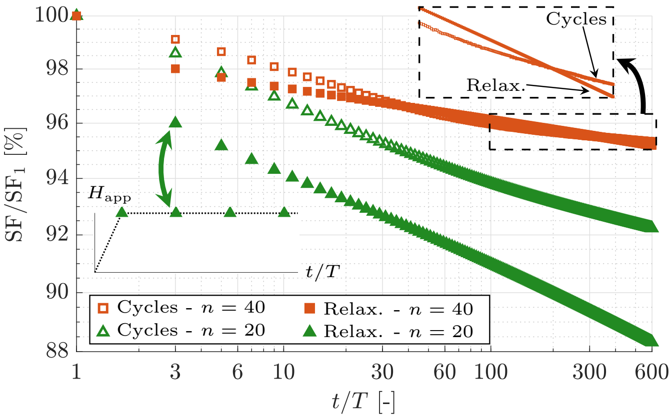

Fig. 6. Relative time evolution of SF at $(y, z) = (0, 4.7)$ mm over a long run in two families of applied field (screen made of the bulk alone): 'cycles' (open symbols), as shown in the inset of Fig. 5 and 'relaxation' (full symbols) as shown in the left inset here. For both families, $n = 20$ (green triangles) and $n = 40$ (red squares) are compared, and $\mu_0 H_{\rm max} \approx 480$ mT ($T = 400$ s). The reference $\rm SF_1$ is $\rm SF(t/T = 1)$. The axes are in logarithmic scale.

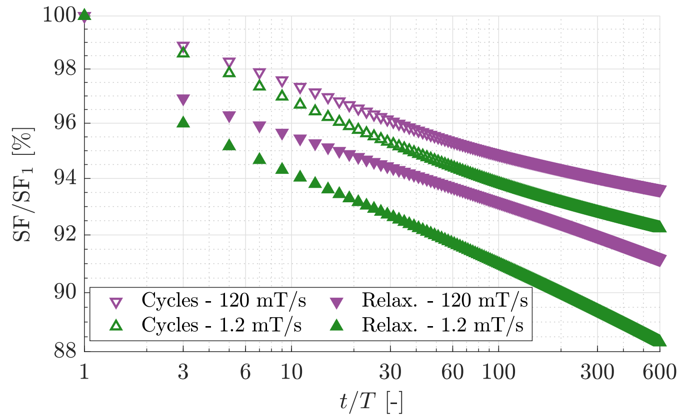

Fig. 7. Relative time evolution of SF at $(y, z) = (0, 4.7)$ mm over a long run in two families of applied field (screen made of the bulk alone): 'cycles' (open symbols) and 'relaxation' (full symbols). For both families, $\mu_0 {\rm d}H_{\rm app}/{\rm d}t = 120$ mT/s ($T = 4$ s, violet downward triangles) and $\mu_0 {\rm d}H_{\rm app}/{\rm d}t = 1.2$ mT/s ($T = 400$ s, green upward triangles) are compared, and $\mu_0 H_{\rm max} \approx 480$ mT and $n = 20$. The reference $\rm SF_1$ is $\rm SF(t/T = 1)$. The axes are in logarithmic scale.

and then reduce over time following (1). For example, at $t_N = (2N + 1)T$, $N \geq 1$ and integer, J induced during the first increasing ramp is around $J(0) - J(0)/n \ln(2NT/\tau_0)$ and J induced during the first decreasing ramp is around $-J(0) + J(0)/n \ln((2N - 1)T/\tau_0)$. Hence, the resulting average $J(t_N)$, is the sum of all the contributions with their sign, i.e.,

$$J_{\rm cycles}(t_N) \approx J(0) - \frac{J(0)}{n} \ln\left(2N \prod_{i=1}^{N-1} \frac{2i}{2i+1}\right). \quad (2)$$

By contrast, in the 'relaxation' case, the average $J(t_N)$ simply writes

$$J_{\rm relaxation}(t_N) \approx J(0) - \frac{J(0)}{n} \ln\left(2N \frac{T}{\tau_0}\right). \quad (3)$$

Since $T > \tau_0$ in (3) and that the product in (2) is smaller than 1, one finds that $J_{\rm cycles}(t_N) > J_{\rm relaxation}(t_N)$ and, indirectly, $\rm SF_{cycles}(t_N) > SF_{relaxation}(t_N)$. Intuitively, this can be understood because $J_{\rm relaxation}$ continuously decreases over time, while $J_{\rm cycles}$ it is periodically 'refreshed' by new currents originating from the successive increasing ramps.

Finally, while all the previous numerical results considered the same sweep rate of $\mu_0 {\rm d}H_{\rm app}/{\rm d}t = 1.2$ mT/s at the bottom of the bulk, the effect of a much faster sweep rate, e.g. 120 mT/s, can be studied. Fig. 7 shows the relative decrease of SF at each occurrence of $H_{\rm max}$ in the 'cycles' case (open symbols) and in the 'relaxation' case at the same time instants (full symbols). In both cases, $\mu_0 H_{\rm max} \approx 480$ mT and $n = 20$, $\mu_0 {\rm d}H_{\rm app}/{\rm d}t = 120$ mT/s ($T = 4$ s, violet downward triangles) and $\mu_0 {\rm d}H_{\rm app}/{\rm d}t = 1.2$ mT/s ($T = 400$ s, green upward triangles, same as in Fig. 6) are compared.

The first observation in Fig. 7 is that, as previously explained, the decay of SF in the 'cycles' case is smaller than in the 'relaxation' case, for both sweep rates. The second observation is that the faster the sweep rate, the smaller the decay of SF. This can be understood as follows. A faster sweep rate results in a higher induced electric field, through Faraday's law, and thus a higher current density J. The consequence of this higher J is that, for a given $H_{\rm max}$, the sample is less penetrated. Since less-penetrated samples are characterized by a smaller relaxation rate [28], it implies that a faster sweep rate results in a smaller relative decay of SF, even in the 'cycles' case.

V. Conclusion

In this work, we studied the behavior of high-temperature superconducting screens subjected to several cycles of inhomogeneous applied field. The key messages are as follows.

(i) For two screens (bulk or hybrid), it was found experimentally that the SF distributions measured after 1 to 30 increasing ramps of applied field are similar.

(ii) Numerically, we observed that the initial SF drops by 2.3% (resp. 13%) when it first reaches $\mu_0 H_{\rm max} = 120$ mT (resp. 480 mT) at the bottom of the bulk screen. By contrast, the relative SF decay for the next 300 cycles (when $H_{\rm app} = H_{\rm max}$) is less than 1% (resp. 5%).

(iii) If $n = \infty$, the J distribution in the bulk at each occurrence of $H_{\rm max}$ would be exactly the same. In practice, the slight decrease of SF between successive cycles results from the small current relaxation (flux creep) arising because n is finite. Remarkably, the decay occurring for successive cycles of applied field is smaller than the decay occurring for conventional current relaxation under $H_{\rm app} = H_{\rm max}$. Also, increasing ${\rm d}H_{\rm app}/{\rm d}t$ leads to a smaller SF decay.

This work therefore validates experimentally and numerically that the screening properties of HTS screens optimized for the first ramp can be maintained throughout the further cycles used in applications.

References

[1] C. C. Chow, M. D. Ainslie, and K. Chau, "High temperature superconducting rotating electrical machines: An overview," *Energy Rep.*, vol. 9, pp. 1124–1156, 2023.

[2] K. S. Haran, D. Loder, T. O. Deppen, and L. Zheng, "Actively shielded high-field air-core superconducting machines," *IEEE Trans. Appl. Supercond.*, vol. 26, no. 2, pp. 98–105, 2016.

[3] R. Sugouchi, M. Komiya, S. Miura, M. Iwakuma, K. Yoshida, T. Sasayama, T. Yoshida, K. Yamamoto, Y. Sasamori, H. Honda, Y. Hase, M. Shuto, M. Konno, and T. Izumi, "Conceptual design and electromagnetic analysis of 2 MW fully superconducting synchronous motors with superconducting magnetic shields for turbo-electric propulsion system," *IEEE Trans. Appl. Supercond.*, vol. 30, no. 4, pp. 1–5, 2020.

[4] N. Rotheudt, M. Fracasso, P. Vanderbemden, and L. Gozzelino, "Superconductor-based passive shielding and screening systems," *Supercond. Sci. Technol.*, vol. 38, no. 4, p. 043002, 2025.

[5] Z. Zhong and W. Wu, "High temperature superconducting closed-loop coils: constructures, key technologies, applications, and future suggestions," *Supercond. Sci. Technol.*, vol. 38, no. 3, p. 033002, 2025.

[6] H. Dong, D. Huang, T. Wang, H. Gu, and F. Ding, "A novel jointless coil: promising unprecedented magnetic field stability to solve the persistent current mode issue in 2G-HTS magnet application," *Supercond. Sci. Technol.*, vol. 37, no. 1, p. 015003, 2023.

[7] N. Rotheudt, S. Brialmont, J.-F. Fagnard, T. Hlasek, J. Plechacek, and P. Vanderbemden, "Improving the screening ability of high-temperature superconductors by combining disk-shaped bulks and closed-loop coated conductors," *Supercond. Sci. Technol.*, vol. 37, no. 6, p. 065008, 2024.

[8] N. Rotheudt, J.-F. Fagnard, T. Hlasek, J. Plechacek, and P. Vanderbemden, "Design rules to scale-up magnetic screens made of bulk superconductors and closed-loop coated conductors: modelling and experiments," *Supercond. Sci. Technol.*, vol. 38, no. 2, p. 025012, 2025.

[9] C. Navau, A. Sanchez, E. Pardo, D.-X. Chen, E. Bartolomé, X. Granados, T. Puig, and X. Obradors, "Critical state in finite type-II superconducting rings," *Phys. Rev. B*, vol. 71, p. 214507, 2005.

[10] L. Wéra, J.-F. Fagnard, K. Hogan, B. Vanderheyden, and P. Vanderbemden, "The influence of an initial trapped field on the magnetic shielding performance of bulk high-temperature superconducting tubes," in *High-Temperature Superconductors: Occurrence, Synthesis and Applications*, M. Miryala and M. Koblischka, Eds. Nova Science, New-York, Etats-Unis, 2018, pp. 75–94.

[11] N. Rotheudt, J.-F. Fagnard, P. Harmeling, and P. Vanderbemden, "Adapting a commercial integrated circuit 3-axis Hall sensor for measurements at low temperatures: Mapping the three components of B in superconducting applications," *Cryogenics*, vol. 133, p. 103693, 2023.

[12] T. Motoki, Y. Yanai, K. Nunokawa, and J. Shimoyama, "Fabrication of high-performance YBa2Cu3Oy melt-textured bulks with selective grain growth," *Appl. Phys. Express*, vol. 13, no. 9, p. 093002, 2020.

[13] T. Motoki, R. Sasada, T. Tomihisa, M. Miwa, S. Nakamura, and J. Shimoyama, "Development of homogeneous and high-performance rebco bulks with various shapes by the single-direction melt growth (SDMG) method," *Supercond. Sci. Technol.*, vol. 35, no. 9, p. 094003, 2022.

[14] F. Antončík, M. Lojka, T. Hlásek, D. Sedmidubský, J. Baumann, J. H. Durrell, D. A. Cardwell, and O. Jankovský, "Novel approach for manufacture of single-grain EuBCO/Ag bulk superconductors via modified single-direction melt growth," *J. Am. Ceram. Soc.*, pp. 1–11, 2023.

[15] G. A. Levin, P. N. Barnes, J. Murphy, L. Brunke, J. D. Long, J. Horwath, and Z. Turgut, "Persistent current in coils made out of second generation high temperature superconductor wire," *Appl. Phys. Lett.*, vol. 93, no. 6, p. 062504, 2008.

[16] H.-G. Lee, J.-G. Kim, S.-W. Lee, W.-S. Kim, S.-W. Lee, K.-D. Choi, G.-W. Hong, and T.-K. Ko, "Design and fabrication of permanent mode magnet by using coated conductor," *Phys. C: Supercond. Appl.*, vol. 445-448, pp. 1099–1102, 2006.

[17] J. Sheng, M. Zhang, Y. Wang, X. Li, J. Patel, and W. Yuan, "A new ring-shape high-temperature superconducting trapped-field magnet," *Supercond. Sci. Technol.*, vol. 30, no. 9, p. 094002, 2017.

[18] Y. Zheng, Y. Wang, J. Li, and Z. Jin, "Magnetization of the joint-free high temperature superconductor (RE)Ba2Cu3Ox coil by field cooling," *AIP Adv.*, vol. 7, no. 9, 2017, 095218.

[19] M. Z. Ali, J. Zheng, F. Huber, Z. Zhang, W. Yuan, and M. Zhang, "4.6 T generated by a high-temperature superconducting ring magnet," *Supercond. Sci. Technol.*, vol. 33, no. 4, p. 04LT01, 2020.

[20] C. Zhao, J. Shi, J. Sheng, and W. Chen, "Study on the electromagnetic characteristics of ring-shaped superconducting permanent magnets for medical applications," *Crystals*, vol. 12, no. 10, p. 1438, 2022.

[21] "Life-hts: Liege university finite element models for high temperature superconductors," https://www.life-hts.uliege.be.

[22] J. Z. Sun, C. B. Eom, B. Lairson, J. C. Bravman, and T. H. Geballe, "Magnetic relaxation, current-voltage characteristics, and possible dissipation mechanisms for high-T_c superconducting thin films of Y-Ba-Cu-O," *Phys. Rev. B*, vol. 43, pp. 3002–3008, 1991.

[23] A. Bossavit and J. Verite, "The "TRIFOU" code: Solving the 3-D eddy-currents problem by using h as state variable," *IEEE Trans. Magn.*, vol. 19, no. 6, pp. 2465–2470, 1983.

[24] J. Dular, C. Geuzaine, and B. Vanderheyden, "Finite-element formulations for systems with high-temperature superconductors," *IEEE Trans. Appl. Supercond.*, vol. 30, no. 3, pp. 1–13, 2020.

[25] C. P. Bean, "Magnetization of hard superconductors," *Phys. Rev. Lett.*, vol. 8, pp. 250–253, 1962.

[26] D. Cardwell, M. Murakami, M. Zeisberger, W. Gawalek, R. Gonzalez-Arrabal, M. Eisterer, H. Weber, G. Fuchs, G. Krabbes, A. Leenders, H. Freyhardt, X. Chaud, R. Tournier, and N. Hari Babu, "Round robin measurements of the flux trapping properties of melt processed Sm–Ba–Cu–O bulk superconductors," *Phys. C: Supercond.*, vol. 412-414, pp. 623–632, 2004.

[27] E. Zeldov, N. M. Amer, G. Koren, A. Gupta, M. W. McElfresh, and R. J. Gambino, "Flux creep characteristics in high-temperature superconductors," *Appl. Phys. Lett.*, vol. 56, no. 7, pp. 680–682, 1990.

[28] I. M. Babich, G. P. Mikitik, and E. H. Brandt, "Magnetic relaxation in partly penetrated critical states of type-II superconductors," *Phys. Rev. B*, vol. 68, p. 052509, 2003.